Tribology Transactions
Publication details, including instructions for authors and subscription information:
http://www.informaworld.com/smpp/title~content=t713669620

The Frictional Behavior of Thin Halide Films on Iron

Feng Gao [a]; Peter V. Kotvis [a]; W. T. Tysoe [a]
[a] Department of Chemistry and Laboratory for Surface Studies University of Wisconsin-Milwaukee, Milwaukee, Wisconsin

First Published on: 01 April 2004
To cite this Article: Gao, Feng, Kotvis, Peter V. and Tysoe, W. T. (2004) 'The Frictional Behavior of Thin Halide Films on Iron', Tribology Transactions, 47:2, 208 - 217
To link to this article: DOI: 10.1080/05698190490431894
URL: http://dx.doi.org/10.1080/05698190490431894

Tribology Transactions, 47: 208-217, 2004

ISSN: 0569-8197 print / 1547-397X online
DOI: 10.1080/05698190490431894

The Frictional Behavior of Thin Halide Films on Iron

FENG GAO, PETER V. KOTVIS and W. T. TYSOE
Department of Chemistry and Laboratory for Surface Studies
University of Wisconsin-Milwaukee
Milwaukee, 53211 Wisconsin

The frictional behavior of thin (<1 μm) sodium chloride, potassium chloride, and potassium iodide films deposited onto iron has been measured in ultrahigh vacuum. It has been shown previously that the friction coefficient decreases from the value for clean iron (∼2) to a minimum when the surface is covered by a monolayer film, and this is referred to as regime one. A second regime is identified in this work for films up to 0.3 μm thick, where the friction coefficient increases with film thickness due to the increased contact area with the rough tribopin. The friction coefficient in this regime obeys Amontons' law. A third regime is found for films thicker than 0.3 μm when the pin is completely supported by the film. Here, the contact behaves elastically, leading to a friction coefficient that varies as $\sqrt{(film\ thickness)}$*. Amontons' law is no longer obeyed in this regime where now the friction coefficient is proportional to* $1/\sqrt{(normal\ load)}$*.*

KEY WORDS

Friction Testing; Solid Lubrication; Iron; Film Thickness; Contact of Rough Surfaces; Vacuum; Surface Films/Coatings

INTRODUCTION

A significant amount of work has been carried out to examine the properties of thin metallic and inorganic films deposited onto harder surfaces (Bowden and Tabor *(1)*; Finken *(2)*; Dayson *(3)*; Liu, et al. *(4)*). The aim of these films is to lower the interfacial friction coefficient, with the assumption that the contact area remains relatively small since the load is supported by the hard substrate, while the lateral force equals the contact area multiplied by the shear strength of the film. Since the shear strength of the softer film is lower than that of the substrate, it has been suggested that this leads to a reduction in friction coefficient (Bowden and Tabor *(1)*). This notion was first demonstrated experimentally by the classical work of Bowden and Tabor, who showed that a ∼1-μm-thick film of indium deposited onto tool steel reduced the friction coefficient from more than 0.3 to less than 0.1 (Bowden and Tabor *(5)*). Further deposition of indium with film thicknesses of up to ∼30 μm caused the friction coefficient to increase once again, presumably because the contact area increased due to the presence of a thicker film of the softer indium. It has also been found that Amontons' law is no longer obeyed for thicker films where the friction coefficient decreases with increasing applied load (Bowden and Young *(6)*; Singer, et al. *(7)*). The theories explaining these results can be broadly classified into ones that consider the contact to behave elastically (Singer, et al. *(7)*; El-Sherbury and Halling *(8)*; Leverson *(9)*; Tian and Saka *(10)*; Matthewson *(11)*; Rabinowicz *(12)*; El Shafei, et al. *(13)*) and those that explore the effects of surface roughness (Finken *(2)*, *(14)*; Dayson *(3)*; Zhang and Kato *(15)*; Ogilvy *(16)*).

As pointed out by Rabinowicz *(12)*, the problem of studying the frictional properties of thin films is plagued by additional experimental problems beyond just measuring the friction coefficient of uncoated surfaces, since the task of maintaining sample cleanliness and depositing clean, well-characterized films becomes exceedingly difficult. To obviate this problem, the experiments described below to measure the tribological properties of thin films have been carried out in ultrahigh vacuum. In this case, the background pressure is $\sim 2 \times 10^{-10}$ Torr, and thus allows a pure, atomically clean substrate to be prepared and a pure thin film to be deposited onto this substrate and frictional properties to be measured without intervening exposure to air (Wu, et al. *(17)*). Experiments have previously been carried out on atomically thin halide layers deposited onto clean iron substrates. These experiments have revealed that low-shear-strength halide films do indeed reduce the interfacial friction coefficient and that this reduction is associated with the *complete* coverage of the surface with a very thin layer (a few Ångstroms thick) of the halide (Wu, et al. *(17)*; Gao, et al. *(18)-(21)*). These results were confirmed by measuring the relative area of the halide film compared to the bare metal surface by exploiting the fact that certain molecules chemisorb strongly on the clean iron surface, but not on the halide (Gao, et al. *(18)*, *(19)*). These experiments were carried out by chemisorbing deuterium on the bare iron surface and confirmed that the initial reduction in friction coefficient was indeed due to the complete coverage of the iron substrate by the halide layer. The point at which this occurs coincides with an increase in the contact resistance, but this does not become infinite until much thicker films have been deposited. This implies that either the tips of some asperities can penetrate the "monolayer" film, but that this does not have a strong influence on the friction coefficient, or that the monolayer film itself can conduct and the contact resistance measurements are probing the formation of a thicker film. It has also

Manuscript received by STLE May 16, 2003
Final manuscript approved December 10, 2003
Review led by Robert Fusaro

NOMENCLATURE

β	$\approx 2R$
α	= proportionality constant between shear strength and pressure
A_C^f	= contact area with the film
A_C^s	= contact area with the substrate
B	= ball radius
c	= 1/2B
d	= separation of contacting rough surfaces
E	= composite elastic modulus
G	= shear modulus
H_f	= hardness of the film material
H_s	= hardness of the substrate material
ν	= Poisson ratio
L	= applied load
σ	= constant in exponential asperity height distribution
p	= t/σ
r	= H_f/H_s
R	= radius of curvature of the tip of an asperity
S_0	= shear strength at zero pressure
t	= film thickness
w	= asperity tip penetration
μ	= friction coefficient in the presence of a film of thickness t
μ_0	= friction coefficient of a monolayer film

been found that the friction coefficients of these films remain almost constant relative to the large initial drop, up to thicknesses of ~2000 Å. In this work, we explore the frictional properties of relatively much thicker halide films, up to ~10,000 Å (1 μm).

EXPERIMENTAL

Experiments were carried out in a stainless steel, ultrahigh vacuum chamber operating at a base pressure of $\sim 2 \times 10^{-10}$ Torr following bake out, which has been described in detail elsewhere (Wu, et al. *(17)*). The chamber is equipped with an ultrahigh-vacuum-compatible tribometer that simultaneously measures normal and lateral forces and the contact resistance between the tip and substrate. It also contains a single-pass, cylindrical-mirror analyzer for Auger analysis of the surface, a quartz crystal microbalance for measuring the thickness of the deposited film, an argon-ion bombardment source for sample cleaning, and an evaporation source for the deposition of inorganic materials. This source has been described in detail elsewhere (Wytenburg and Lambert *(22)*). The potassium chloride, potassium iodide, and sodium chloride (Alfa Aesar, 99.99% purity) were loaded into the small alumina tube furnace of the evaporation source and outgassed in ultrahigh vacuum prior to use. The clean iron foil sample (0.1 mm thick, Aldrich, 99.999% pure) was attached to a sample manipulator where it was mounted onto a steel plate (0.5 mm thick) to provide a rigid base for the tribological measurements. Prior to mounting onto the steel plate, the sample was polished with 1 μm diamond paste to a mirror finish. The sample can be resistively heated and cleaned using ion bombardment to remove any impurities (primarily carbon, chlorine, and sulfur) and annealed to 1000 K prior to carrying out any tribological measurements. The iron sample following this treatment is almost atomically smooth, and no significant surface features can be discerned using atomic force microscopy (AFM). The hemispherical tribopin (6.35×10^{-3} m radius) was made from tungsten carbide containing some cobalt binder. This is cleaned by electron beam heating via a retractable filament that can be placed in front of the pin. An Auger analysis of the pin following this treatment was in accord with the bulk structure. Measurement of the pin topology using AFM shows that it is substantially rougher than the iron substrate (Wu, et al. *(17)*). AFM images of the tribopin were collected ex situ using a scanning probe microscope. The data were analyzed using NIH Image software (National Institutes of Health *(23)*). Frictional measurements were carried out using a pin-on-flat configuration with a single linear pass on a freshly prepared film at a sliding speed of 4×10^{-3} m/s. Experiments were generally carried out using an applied load of 0.29 N, yielding a maximum Hertzian stress of 420 MPa.

RESULTS

Pin Surface Topology

As noted above, AFM images of the substrate showed it to be much smoother than the tribopin so that the overall roughness of the interface is controlled by the topology of the tribopin. As has been pointed out elsewhere (Zhang and Kato *(15)*), this situation is analogous to the contact of two rough surfaces. It is, however, simpler to theoretically analyze a situation in which one surface is taken to be smooth and the other rough. The topology of the tribopin measured using AFM is shown in Fig. 1. This reveals the presence of a number of asperities of varying heights on the surface, and the shape of the tips of the asperities appears to be approximately paraboloidal in shape. The root-mean-square roughness of the surface is 0.12 ± 0.01 μm so that more than 95% of the surface lies within a distance of ~0.3 μm (see Fig. 8). The images were analyzed to measure the total number of asperity peaks with a height larger than some value d, where d is the vertical height from the surface. It has been suggested that, for a randomly rough surface, the number of asperity peaks between z and $z + \delta z$ is described by a Gaussian distribution (Johnson *(24)*; Greenwood and Williamson *(25)*). A major drawback to this function is that it cannot be analytically integrated between defined limits. This is not a major limitation when studying uncoated surfaces since much information concerning the nature of the contact can be obtained without having to evaluate the integrals. However, in order to analyze film-covered surfaces, it is necessary to integrate the peak height distribution in order to obtain an analytical function that can be fit to the experimental data. In many cases, it is not necessary to have a full asperity height distribution since only the tips of asperities penetrate the surface of the film. In these cases, an exponential distribution has been used (Johnson *(24)*), where the number of asperity peaks lying at a height between z and $z + \delta z$ is proportional to $\exp(-z/\sigma)dz$. Simple integration shows that the total number of asperities higher than some value d is proportional

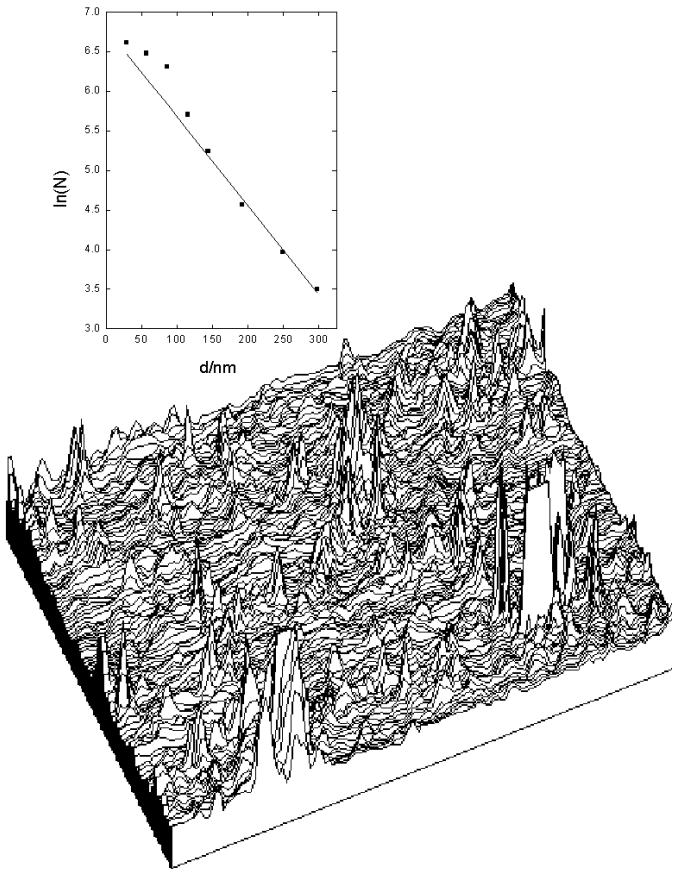

Fig. 1—The topology of the tungsten carbide tribopin measured using AFM showing a region 24.6 × 24.6 μm^2. Shown as an inset is a plot of ln(*N*) versus *d*, where *N* is the total number of asperity tips of a height larger than *d*.

to $\exp(-d/\sigma)$. The number of peaks N, higher than some value d, is measured from the AFM images and $\ln(N)$ is plotted versus d in the inset of Fig. 1. This plot is linear over the range measured indicating that the exponential distribution is a good approximation to the true topology. The value of σ in this exponential function, measured from the slope, yields $\sigma = 89 \pm 5$ nm.

Friction Coefficient as a Function of Film Thickness

It has been shown previously that the friction coefficient of clean iron measured using the tungsten carbide tribopin in ultrahigh vacuum, which has a value of ~2, decreases rapidly to a limiting value when the surface is covered by a monolayer of a halide (Wu, et al. *(17)*; Gao, et al. *(18)-(21)*). This limiting friction coefficient depends on the nature of the halide film (Gao, et al. *(20)*). The friction coefficient changes only slightly compared to this initial large drop with the addition of more halide. However, since friction coefficients have been found previously to increase at larger film thicknesses after having reached their minimum values (Bowden and Tabor *(1)*, *(5)*), the frictional behavior of thicker films up to ~1 μm has been explored. The variation in friction coefficient as a function of film thickness for potassium iodide deposited onto clean iron is displayed in Fig. 2, collected using an applied load of 0.29 N. We have not included the large initial drop from the clean surface value in order to allow the smaller changes occurring with the thicker films to be more easily seen. Thus, the "initial" friction coefficient of 0.2 at low film thicknesses corresponds to the decrease caused by the completion of the first monolayer, which occurred after a potassium iodide film of total average thickness ~4 nm had been deposited (Gao, et al. *(20)*). These data show that the friction coefficient increases as the film becomes thicker, in general agreement with observations for indium on steel (Bowden and Tabor *(1)*, *(5)*). It is evident that the initial increase as a function of film thickness t (for small values of t) varies as t^n where $n > 1$, while at higher film thicknesses, a similar power dependence will result in a value of $n < 1$. The data are fit to a simple power law $\mu \propto t^n$, where a $t^{3/2}$ dependence is shown for the data for small film thicknesses (<0.3 μm). The agreement between experiment and theory is excellent up to a total film thickness of 0.3 μm, while there are substantial differences between the theoretical prediction and the experimental data above this value. A fit to a $t^{1/2}$ power law is shown at higher film thicknesses and shows good agreement with the experimental data. These power-law dependencies will be discussed in greater detail below. However, the vertical projection of the contact area A' for a paraboloid asperity contact, which penetrates a distance t, varies as $t^{3/2}$. Realizing that the plowing contribution to the friction force depends on A' (Bowden and Tabor *(1)*) immediately suggests that the increase in friction coefficient with film thickness may be due to plowing. However, as will be seen later, this turns out not to be the case.

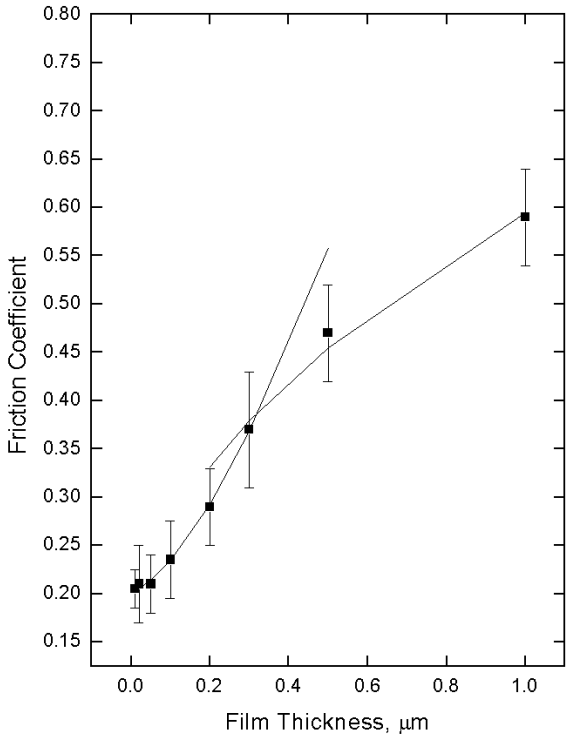

Fig. 2—Plot of friction coefficient versus film thickness for potassium iodide deposited onto clean iron in ultrahigh vacuum for film thicknesses greater than 0.01 μm where the data were collected using an applied load of 0.29 N and a sliding speed of 4×10^{-3} m/s. The lines through the data correspond to a polynomial fit to the data (see text).

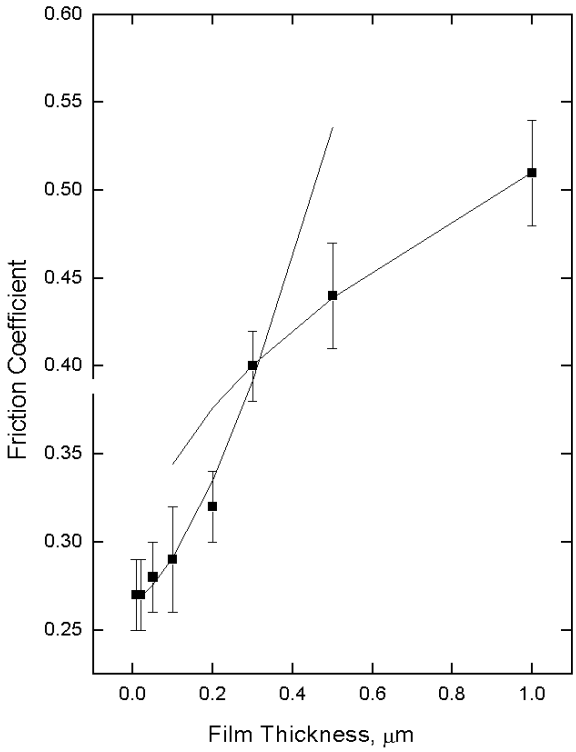

Fig. 3—Plot of friction coefficient versus film thickness for potassium chloride deposited onto clean iron in ultrahigh vacuum for film thicknesses greater than 0.01 μm where the data were collected using an applied load of 0.29 N and a sliding speed of 4×10^{-3} m/s. The lines through the data correspond to a polynomial fit to the data (see text).

Similar plots and the fits of the data to power laws are shown in Fig. 3 for potassium chloride friction coefficients as a function of film thickness collected using an applied load of 0.29 N, where again the plot is started at the limiting value of the friction coefficient found following the deposition of the first monolayer (0.27). These data show an asymptotic limit of friction coefficient of 0.5 to 0.6 at very large film thicknesses. The friction coefficient of a KCl disk has been measured in ultrahigh vacuum (Wu, et al. *(17)*) and found to be ~0.3. It would be expected that the friction coefficient of very thick films should tend to the value of the bulk material. In this case, although the friction coefficient was measured in ultrahigh vacuum after the chamber had been baked, because the thick potassium chloride disk is insulating, standard ultrahigh vacuum cleaning techniques, for example ion bombardment, could not be used. In contrast, the potassium chloride that is evaporated onto the surface had been outgassed in ultrahigh vacuum prior to deposition and has been shown by X-ray photoelectron spectroscopy (XPS) (Wu, et al. *(17)*) and X-ray diffraction (XRD) (Gao, et al. *(20)*) to result in the deposition of a pure film. It appears, therefore, that the potassium chloride disks may have been contaminated, and this emphasizes the difficulty of obtaining clean samples for tribological measurements and the effect that small amounts of contamination can have on the friction coefficient.

Finally, a similar set of data for the friction coefficient of sodium chloride as a function of film thickness collected using an applied load of 0.29 N is shown in Fig. 4. Again, the limiting friction coefficient for very thin films (~0.49) also corresponds to the value after the completion of the first monolayer. The data are fit to the same power laws as the potassium iodide (Fig. 2) and chloride (Fig. 3) data and yield similarly good fits for sodium chloride. The friction coefficient of freshly cleaved sodium chloride against clean steel is between 0.7 and 0.8 (Bowden and Tabor *(1)*), which is in much better agreement with the asymptotic value for the deposited films shown. Presumably, the surfaces remain reasonably clean for some period after cleavage.

The general behavior of the friction coefficient as a function of film thickness for all of the films is strikingly similar. In all cases, the friction coefficient varies as $t^{3/2}$ for films thinner than 0.3 μm and as $t^{1/2}$ for thicker films. There appears, therefore, to be a change in frictional behavior at a critical film thickness of 0.3 μm independent of the mechanical properties of the film. The results presented above can be obtained repeatedly on freshly prepared samples, implying that the topology of the hard tungsten carbide pin is not appreciably affected by repeated rubbing against the soft substrate. This conjecture is confirmed by AFM measurements made after carrying out several tribological experiments, which showed no change in the surface roughness of the tribopin.

Friction Coefficient as a Function of Load

The friction coefficients as a function of applied load are plotted in Fig. 5 for potassium iodide, Fig. 6 for potassium chloride, and Fig. 7 for sodium chloride. In all cases, the friction coefficient is

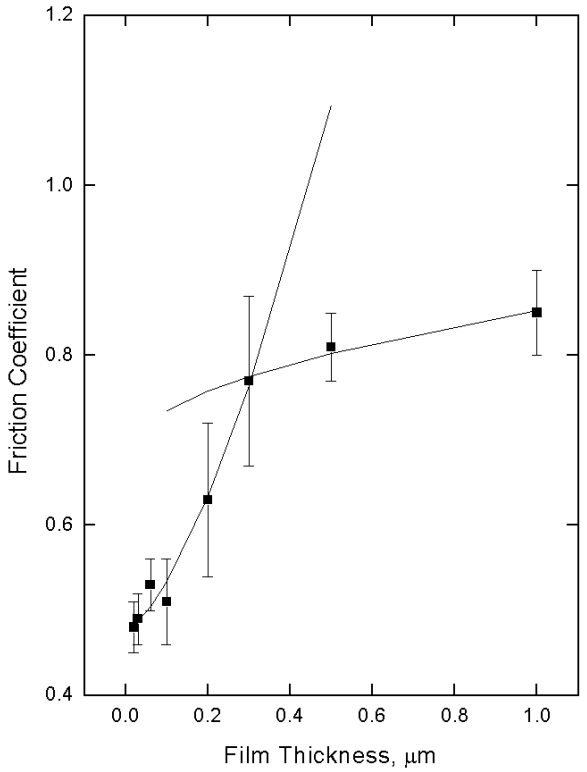

Fig. 4—Plot of friction coefficient versus film thickness for sodium chloride deposited onto clean iron in ultrahigh vacuum for film thicknesses greater than 0.01 μm where the data were collected using an applied load of 0.29 N and a sliding speed of 4 $\times$ 10^{-3} m/s. The lines through the data correspond to a polynomial fit to the data (see text).

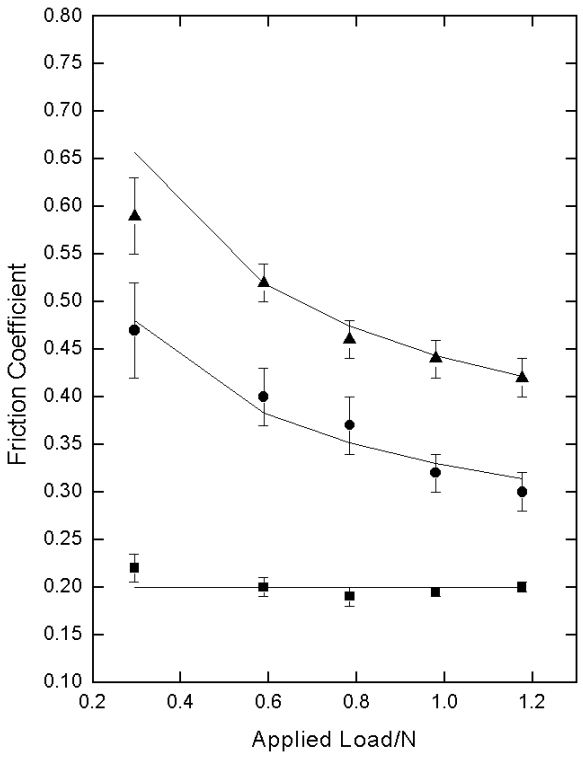

Fig. 5—Plot of friction coefficient versus applied load for potassium iodide deposited onto clean iron in ultrahigh vacuum, where the film thicknesses are 0.02 (■), 0.5 (●), and 1.0 (▲) μm using a sliding speed of 4 $\times$ 10^{-3} m/s. A theoretical fit is shown plotted through the data (see text).

independent of applied load for film thicknesses less than 0.3 μm, but decreases with increasing applied load for thicker films. The latter load dependence of the friction coefficient has been fit to a function of the form:

$$\mu = C + \frac{D}{\sqrt{L}} \qquad [1]$$

where C and D are constants and L is the applied load where the fits are shown as solid lines. In all cases, the agreement with the experimental data is excellent and these fits will be discussed in greater detail below.

Friction Regimes as a Function of Film Thickness

The frictional behavior varies in a reasonably complicated manner with film thickness and can be assigned to various thickness regimes as follows.

Regime 1

The first regime is observed for very thin films, generally thinner than 4 to 5 nm where the friction coefficient drops rapidly from the clean-surface value on iron (~2) to a limiting value after the surface has been completely covered by at least a monolayer of the thin film (Wu, et al. *(17)*; Gao, et al. *(18)-(21)*). The resulting friction coefficient obeys Amontons' law and is proportional to the hardness of the film material (Gao, et al. *(20)*).

Regime 2

The second regime occurs after the completion of the first monolayer and for film thicknesses t less than 0.3 μm, where the friction coefficient is empirically found to vary as $t^{3/2}$. Since the upper thickness limit of 0.3 μm is independent of the nature of the film, and since AFM measurements show that this is the distance between the lowest and highest points of the tribopin (see Fig. 8), this suggests that this behavior depends on the morphology of the tribopin. The friction coefficient in this regime also obeys Amontons' law.

Regime 3

The third regime is found for films thicker than 0.3 μm where the friction coefficient is empirically found to vary as $t^{1/2}$ but, in this case, does not obey Amontons' law, where the load dependence of the friction coefficient is given by Eq. [1]. It should be noted that, although a $t^{1/2}$ dependence is shown plotted through the experimental data, a $t^{1/3}$ dependence fits almost as well. Such a dependence strongly indicates that the contact behaves elastically and will be discussed in greater detail below.

DISCUSSION

Three friction regimes have been identified and their characteristics described in the previous section. The first regime is primarily responsible for the rapid reduction in friction and has been associated with the complete coverage of the iron surface with

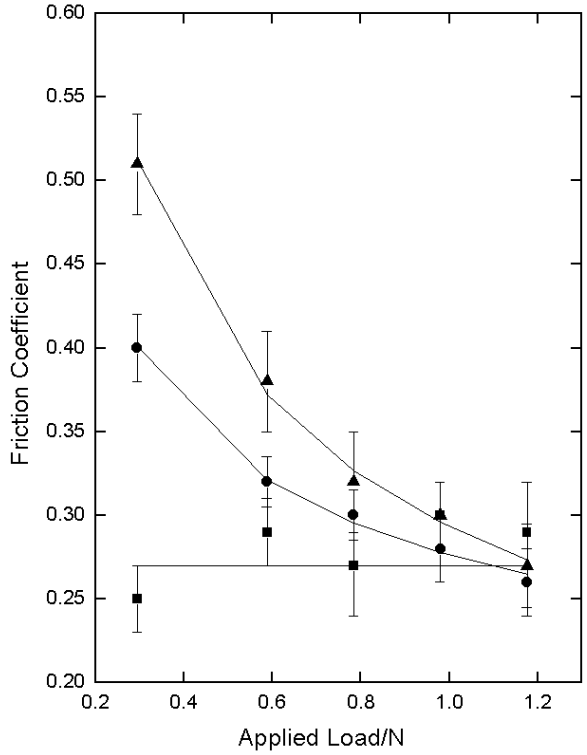

Fig. 6—Plot of friction coefficient versus applied load for potassium chloride deposited onto clean iron in ultrahigh vacuum, where the film thicknesses are 0.05 (■), 0.3 (●), and 1.0 (▲) μm using a sliding speed of 4×10^{-3} m/s. A theoretical fit is shown plotted through the data (see text).

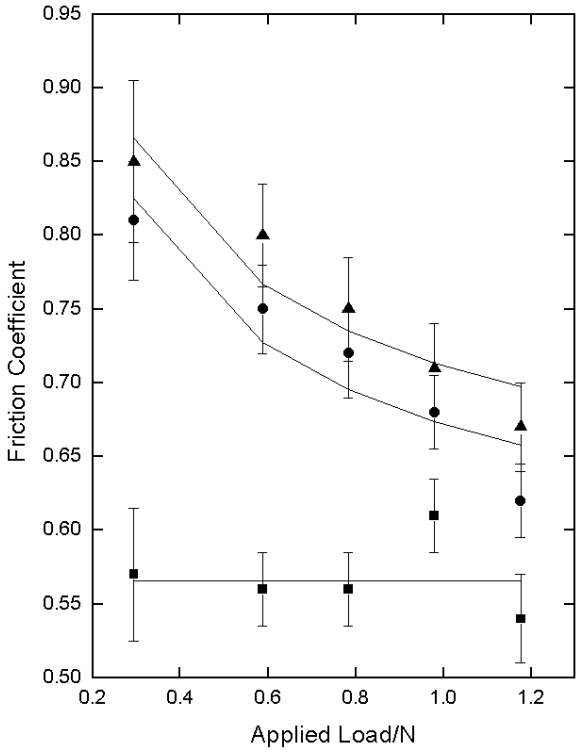

Fig. 7—Plot of friction coefficient versus applied load for sodium chloride deposited onto clean iron in ultrahigh vacuum, where the film thicknesses are 0.1 (■), 0.5 (●), and 1.0 (▲) μm using a sliding speed of 4×10^{-3} m/s. A theoretical fit is shown plotted through the data (see text).

a monolayer film of the halide (Wu, et al. *(17)*; Gao, et al. *(18)-(21)*). Thus, the halide monolayer appears to provide a protective layer that lowers friction. Following the completion of the first monolayer of film, a further increase in film thickness results in an increase in friction coefficient where a power law fit shows a $t^{3/2}$ dependence. This *a priori* implies that plowing contributes to the increase in friction coefficient in this case. It will be found that it is not necessary to invoke plowing to adequately describe the experimental behavior for these thicker films. The observation that the transition from regime 2 to regime 3 occurs at a film thickness of 0.3 μm and is independent of the nature of the film suggests that this is, in fact, controlled by the topology of the tribopin. Further support for this notion comes from measurement of the damage in the iron substrate as a function of film thickness (Gao, et al. *(21)*). In this case, the morphology of the iron surface was examined using AFM after tribological experiments in the presence of a potassium chloride film and where the film had been removed using deionized water. It was found that a potassium chloride film thicker than ~0.2 μm was required to suppress any damage to the iron substrate below, implying that the tips of the asperities on the tribotip could still reach the substrate in the presence of thinner films. This proposal can be further tested by performing similar experiments with tribopins of different roughnesses, and these experiments are underway.

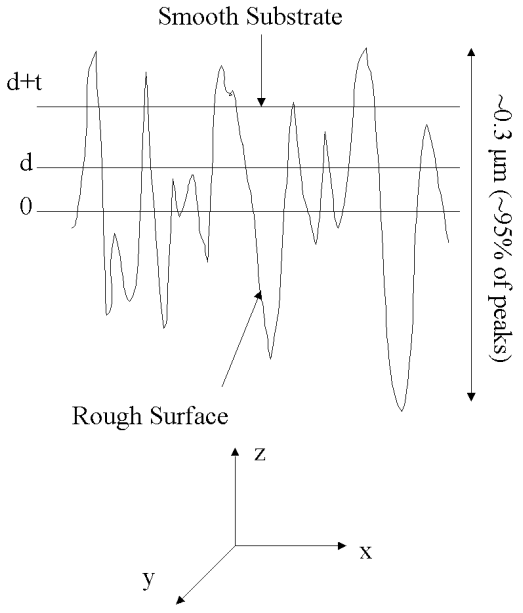

Fig. 8—Schematic diagram of the model for the analysis of a rough surface in contact with a smooth surface covered by a film of thickness *t* where the separation between the smooth surface and the mean of the asperity height distribution is *d*.

The contact behavior between a rough pin and a flat surface in the presence of a film of thickness t is analyzed using the Greenwood-Williamson theory *(25)*. Note that such an analysis between a smooth and rough surface is mathematically equivalent to the contact of two rough surfaces. In this case, the topology of the surface is described in terms of the distribution of the tips of the asperities where the probability that an asperity tip lies between z and $z + \delta z$ is given by $p(z)\,dz$ such that:

$$\int_{-\infty}^{\infty} p(z)dz = 1 \qquad [2]$$

so that the probability distribution is correctly normalized. The contact properties of a thin film in contact with a rough surface have been analyzed previously (Dayson *(3)*), where the contact areas in the substrate and film were determined from a probability distribution that described the height at any point on the surface, not the asperity height distribution, and so is different from a Greenwood-Williamson treatment. In the following, we use a more conventional Greenwood-Williamson approach, but with an exponential peak height distribution function; first since analytical solutions can be obtained, and second, since the measured peak height distribution appears to be well described by an exponential function (Fig. 1). Thus, $p(z)$ is given by:

$$p(z) = \frac{1}{2\sigma} e^{-z/\sigma}, \qquad [3]$$

which has been normalized (Eq. [2]) such that $p(z) = p(-z)$.

The topology of the asperities is closer to paraboloidal than spherical (Fig. 1), so that the surface contour of a tribotip is described by:

$$z = a(x^2 + y^2) \qquad [4]$$

where the z axis is oriented normal to the surface, which defines the $x - y$ plane. In this case, for an asperity tip penetration w the contact area A_C is given by:

$$A_C = \frac{\pi w}{a} \qquad [5]$$

This is written, following Greenwood and Williamson, as:

$$A_C = \beta \pi w \qquad [6]$$

which is exact for a paraboloidal contact. It is straightforward to show that $\beta \approx 2R$ where R is the radius of curvature of the end of the paraboloidal asperity tip assuming that this can be approximated by a hemisphere. The number of asperities per unit area is taken to be N and the total normal pressure P.

The contact geometry is shown in Fig. 8 where d is the separation of the surfaces, which is measured between the mean of the asperity peak height distribution (taken as $z = 0$) and the outermost surface of the film, and t is the film thickness. Thus, again following Greenwood and Williamson, the contact area in the film is given as:

$$A_C^f = N\pi\beta \int_d^{d+t} (z - d)p(z)dz \qquad [7]$$

and the contact area in the substrate by:

$$A_C^s = N\pi\beta \int_{d+t}^{\infty} (z - d)p(z)dz \qquad [8]$$

It should be noted that, since these asperities also penetrate the film, they are also partially supported by it. However, the AFM image of the surface shown in Fig. 1 reveals that the surface of the asperities drops steeply away from the tips so that the area supported by the "shank" of the tip is likely to be small, so that this effect is neglected.

It is also assumed that the contact pressures at the hard asperity tips are sufficiently high that the substrate deforms plastically. This is often assumed to be the case and leads to Amontons' law behavior (Bowden and Tabor *(1)*). If the film material has hardness H_f and the substrate H_s, then the applied load is supported by both the film and the substrate so that:

$$P = \frac{1}{2}\left(H_f A_C^f + H_s A_C^s\right) \qquad [9]$$

where the factor of 1/2 is included following Xie and Williams *(26)* since the applied normal load is carried by the normal pressure, which is equal to H acting on the curved leading face of the hemisphere. The inclusion of this factor, however, does not affect the final result. Since the properties of softer films on harder substrates are of greatest interest, in general $H_f < H_s$. Substituting from Eqs. [7] and [8] yields:

$$P = \frac{N\pi\beta}{2}\left\{H_f \int_d^{d+t} (z - d)p(z)dz + H_s \int_{d+t}^{\infty} (z - d)p(z)dz\right\} \qquad [10]$$

This equation can be solved analytically using the probability distribution of Eq. [3] to yield an analytical function for the separation of the surface as a function of applied pressure P:

$$\frac{d}{\sigma} = \ln\left(\frac{N\pi\beta\sigma[H_f + (H_s - H_f)e^{-t/\sigma}(1 + t/\sigma)]}{4P}\right) \qquad [11]$$

While this is not required explicitly for the clean-surface solutions, it is necessary for the solution of the film-covered surfaces. The value of d can then be used to separately calculate the contact properties of the film and substrate. The contact areas in the film and substrate can be found by evaluating Eqs. [7] and [8], respectively, using the limits of integration given by Eq. [11]. The ratio of the contact area of the substrate, normalized to that of the clean surface, is obtained by evaluating Eq. [8] and normalizing this to the contact area of the film-free surface and is given by:

$$\frac{A_C^s}{A_C^s(t = 0)} = \frac{(1 + p)e^{-p}}{[r + (1 - r)(1 + p)e^{-p}]} \qquad [12]$$

where $p = t/\sigma$ and $r = H_f/H_s$, which is thus less than unity. A similar equation is found for the contact area in the thin film and is given by:

$$\frac{A_C^f}{A_C^s(t = 0)} = \frac{1 - e^{-p}(1 + p)}{[r + (1 - r)(1 + p)e^{-p}]} \qquad [13]$$

These contact areas, relative to that for the clean surface, are plotted for the substrate and the film as a function of t/σ in Fig. 9 for $r = 0.103$. The Knoop hardness of the iron substrate has been measured to be 690 MPa (Wu, et al. *(17)*), while that for potassium chloride is 71 MPa (Moses *(27)*; Musikant *(28)*), yielding the r value for KCl of 0.103 used for the plot in Fig. 9. As expected, at $t = 0$, the relative contact area in the substrate is unity, while that in the (nonexistent) film is zero. It is evident that the contact area in the substrate is relatively unaffected by the presence of

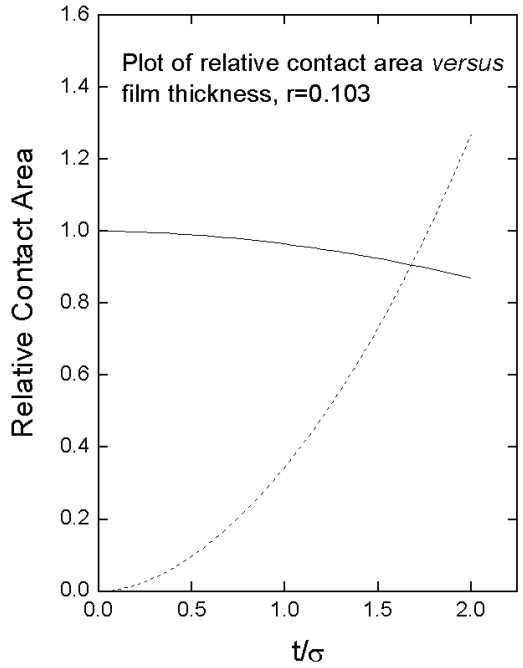

Fig. 9—Theoretical plot of relative contact area in the substrate (solid line) and in a film of thickness *t* (dashed line) as a function of *t*/σ where σ is the constant in the exponential peak height distribution (see text).

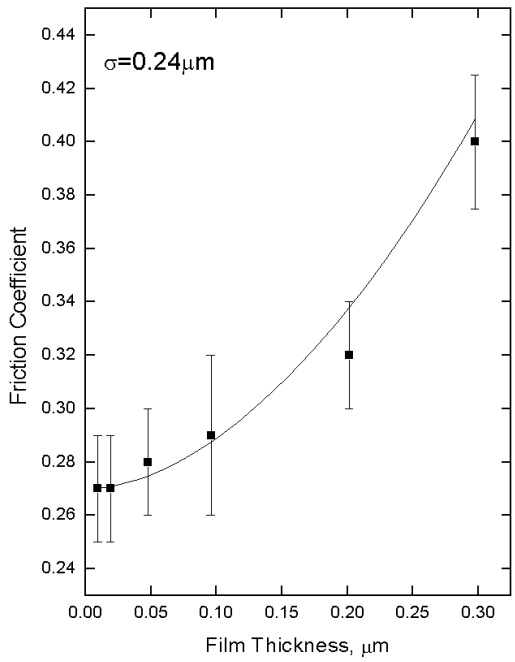

Fig. 10—Comparison of the experimental values of friction coefficient (■) with theoretical predictions (solid line) for the friction of potassium chloride on iron as a function of film thickness using a best-fit value of $\sigma = 0.24$ μm.

the film, while the contact area in the film increases rapidly. This is a direct consequence of the relatively low hardness of the film, which can support only a relatively small load, even for relatively large contact areas.

The simplest interpretation, therefore, for the increase in friction coefficient as the film thickness increases is that this is due to the increased area of the contact, thus requiring an additional force to shear those contacts. In the case of KCl (represented by $r = 0.103$), the friction coefficient decreases from the clean surface value of ~2 to a value of $\mu_0 = 0.27$ when the surface is covered by a monolayer of KCl. This effect is therefore due to sliding of the tribopin against a monolayer of KCl. The simplest assumption is that the sliding of the asperity tips of the tribopin against the film yields a similar friction coefficient as sliding against the monolayer film on the substrate. Since the substrate contact area is almost unaffected by the presence of a halide film up to, at least, $t \sim 2\sigma$ (Fig. 9), this is taken to be constant so that the total friction coefficient is given by:

$$\mu = \mu_0\left(1 + \frac{A_C^f}{A_C^s(t=0)}\right) \qquad [14]$$

where μ_0 is the limiting friction coefficient of the monolayer halide film, which is 0.27 in the case of KCl. Substituting from Eq. [13] into Eq. [14] yields an analytical expression for the friction coefficient as:

$$\mu = \mu_0\left(1 + \frac{1 - e^{-p}(1+p)}{[r + (1-r)(1+p)]e^{-p}}\right) \qquad [15]$$

Again, for a film of KCl, $\mu_0 = 0.27$ and $r = 0.103$. Equation [15] is now fit to the experimental data for films thinner than 0.3 μm by adjusting the value of σ. The best fit is found for $\sigma = 0.24 \pm 0.02$ μm and the comparison between experiment (■) and theory (solid line) is displayed in Fig. 10, where clearly the agreement is extremely good. These results suggest that in region 2 the friction increase is due to the increased contact area between the rough tribopin and the thin film.

A more stringent test of the predictive nature of the theory is to calculate the friction coefficients for potassium iodide and sodium chloride films *without adjustable parameters*. The data used for the calculations are summarized in Table 1. The value of σ is fixed at 0.24 μm, the value of r is calculated from literature values of the hardnesses of the halide (Moses *(27)*; Musikant *(28)*), and μ_0 is taken from previous experiments for thin halide films on iron (Wu, et al. *(17)*; Gao, et al. *(20)*). The resulting plots are shown in Fig. 11(a) for sodium chloride and Fig. 11(b) for potassium iodide. In both cases, the agreement between experiment (■) and theory (solid line) is very good.

The initial power function fits showed that the friction coefficient in this regime varied as $t^{3/2}$ (Figs. 2-4). It turns out that,

TABLE 1—PARAMETERS USED TO CALCULATE THE VARIATION IN FRICTION AS A FUNCTION OF FILM THICKNESS FOR FILMS UP TO 0.3 μM THICK

Material	Hardness/MPa	r [a]	μ_0
KI	49	0.0071	0.220 (Gao, et al. *(18)*)
KCl	71 (100 face)	0.103	0.270 (Wu, et al. *(17)*)
NaCl	179	0.259	0.495 (Gao, et al. *(18)*)

[a] Calculated using a value of 690 MPa for the hardness of iron (Wu, et al. *(17)*).

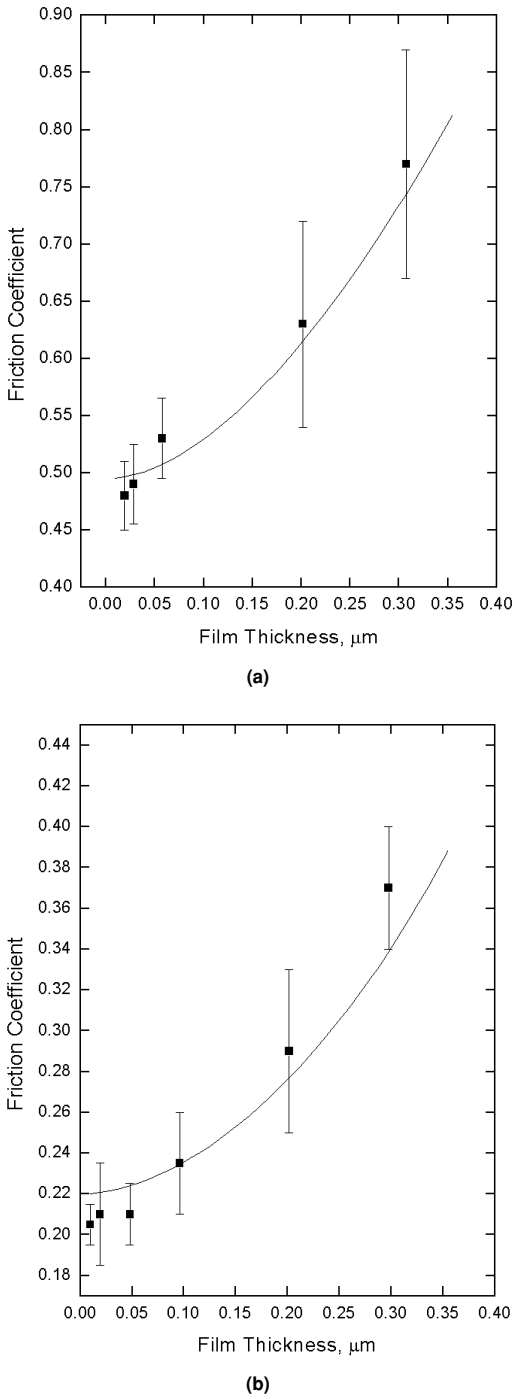

Fig. 11—Comparison of the experimental values of friction coefficient (■) with theoretical predictions (solid line) for the friction of (a) sodium chloride and (b) potassium iodide on iron as a function of film thickness using a value of $\sigma = 0.24$ μm where the other parameters are summarized in Table 1.

coincidentally, the function shown in Eq. [13] varies as approximately $t^{3/2}$ so that this behavior is not indicative of any plowing effects but merely arises from the exponential peak height distribution of the tribopin. Indeed, calculating the plowing force from the area at the front of the asperity tips of the tribopin reveals that it is much smaller than the force due to shear indicating that the friction coefficient appears to arise entirely due to shear at the interface and that plowing makes little contribution to the lateral force. Finally, the theory outlined above is also in accord with the observation that the friction coefficient in regime 2 is independent of the applied load and so obeys Amontons' law.

The frictional behavior changes abruptly when the film thickness exceeds ~0.3 μm and is referred to above as regime 3. The data of Fig. 9 suggest that, because the substrate is much harder than the film, asperities can penetrate the film and the majority of the load is supported by the substrate. However, as the film becomes as thick as the maximum peak-to-valley distance on the surface, material cannot be displaced by the asperities and the surfaces must be separated by the film. As noted above, >95% of the surface height distribution lies within a distance of 0.3 μm (Fig. 8), consistent with the film thickness at which the transition to regime 3 takes place.

Regime 3 is characterized by a load-dependent friction coefficient and a fractional order thickness dependence. This implies that the contact is behaving elastically. Such behavior has been modeled assuming a Hertzian contact (Singer, et al. *(7)*) where the friction coefficient is given by:

$$\mu = \pi S_0 \left(\frac{3B}{4E}\right)^{2/3} L^{-1/3} + \alpha \qquad [16]$$

where the shear strength of the interface is assumed to be pressure dependent and given by:

$$S = S_0 + \alpha P \qquad [17]$$

where P is the pressure in the contact, α a proportionality constant, B the radius of the ball, E the composite elastic modulus of the film, and L the applied load. This was found to reproduce the frictional behavior of thin molybdenum disulfide coatings where α was found to be close to zero, indicating that the shear strength was not pressure dependent over the range of pressures used in the experiment. This theory is applicable to thick films, so does not yield a film thickness dependence. Finken *(2)* proposed an alternative model that resulted in a friction coefficient given by:

$$\mu = KA\sqrt{\frac{t}{L}} \qquad [18]$$

where t is the film thickness and L the applied load. The constant K is a relatively complicated integral but was shown to be close to unity. The constant A is given by:

$$A = \pi S \sqrt{\frac{(1-2\nu)}{\pi G c(1-\nu)}} \qquad [19]$$

where ν is the Poisson ratio of the layer, G its shear modulus, and $c = 1/2B$ where B is the ball radius. Equation [18] predicts that the interfacial friction coefficient should vary as $1/\sqrt{L}$ for fixed values of t, and indeed such behavior is found experimentally (Figs. 5-7). The friction coefficient is also found to vary as $\sqrt{t}$ for fixed loads in regime 3 as shown in Figs. 2-4. It should be mentioned that Eq. [18] predicts that the friction coefficient should tend to zero as t becomes zero and should become infinite as the load tends to zero. In fact, the fits shown in Figs. 2-7 have finite values of the friction coefficient at $t = 0$ and $L = 0$. This may be rationalized by invoking a pressure-dependent shear strength as in Eq. [17].

It is evident that the value of σ used in Figs. 10 and 11 to fit the variation of friction coefficient with film thickness in regime 2 ($\sigma \approx 240$ nm) is substantially larger than the value measured for the tribotip using AFM (Fig. 1, $\sigma = 89 \pm 5$ nm). There may be two origins of this discrepancy. First, the theory developed above assumes that the halide film is not displaced by the asperity tips that penetrate it. If this occurs, the film material displaced by the tips of the asperities on the pin will accumulate within the gaps between the asperities, leading to an effective larger film thickness than that initially deposited. Second, Eq. [14] was written assuming that the frictional behaviors of the thin film and the surface monolayer are identical. This may not be the case, and Eq. [14] can be rewritten by assuming that the film has a different friction coefficient $\mu_f = f\mu_0$ as:

$$\mu = \mu_0 \left(1 + f \frac{A_C^f}{A_C^s(t=0)}\right) \qquad [20]$$

This function can be fit to the frictional data for films thinner than 0.3 μm shown in Figs. 10 and 11 by fixing σ at 89 nm (corresponding to the value measured using AFM, Fig. 1) and by adjusting the value of f. The resulting fits are as good as those shown in Figs. 10 and 11 and yield values of $f \sim 0.14$, 0.15, and 0.26 for KI, KCl, and NaCl respectively. The true situation is likely to be a combination of these effects so that the effective film thickness in the rough contact is likely to be somewhat larger than the deposited film thickness due to material displacement, and the thicker film may have a lower friction coefficient than the monolayer.

When the total film thickness exceeds the total distance between the lowest and highest points on the pin ($\sim$0.3 μm), there is no further space into which the halide film can be displaced so that the pin asperities no longer contact the surface, leading to a rapid transition to regime 3. This notion is corroborated by the observation that damage in the substrate is not suppressed until a film thicker than $\sim$0.2 μm has been deposited (Gao, et al. *(21)*).

CONCLUSIONS

The frictional behavior of thin halide films deposited onto clean iron in ultrahigh vacuum has been measured as a function of film thickness and applied load. It has been shown previously that the friction coefficient falls from its initially high value of $\sim$2 to a limiting lower value when the surface is covered by a monolayer of a halide film. Two additional regimes are identified as the film thickness increases. In regime 2, the friction coefficient increases with increasing film thickness but obeys Amontons' law. This is due to an increase in contact area between a rough tribopin and a thicker halide film. A third regime is identified when the film becomes sufficiently thick that all of the spaces between the asperities of the tribopin are filled with a halide, which occurs when the film is thicker than $\sim$0.3 μm. In this case, the contact behaves somewhat elastically and the friction varies approximately as the square root of the film thickness at constant applied load. Amontons' law is no longer obeyed and the friction coefficient is proportional to $(\text{LOAD})^{-1/2}$ at constant film thickness. These observations are in accord with a theory proposed by Finken *(2)*.

ACKNOWLEDGMENT

We gratefully acknowledge support of this work by the Chemistry Division of the National Science Foundation under grant number CHE-9213988.

REFERENCES

(1) Bowden, F. P. and Tabor, D. (1954), *The Friction and Lubrication of Solids*, Oxford University Press, Oxford.
(2) Finken, E. F. (1969), "A Theory for the Effects of Film Thickness and Normal Load in the Friction of Thin Films," *J. Lubr. Technol.*, **91**, p 551.
(3) Dayson, C. (1971), "The Friction of Very Thin Solid Film Lubricants on Surfaces of Finite Roughness," *ASLE Trans.*, **14**, p 105.
(4) Liu, Z., Neville, A., Reuben, R. L. and Shen, W. (2001), "The Contribution of a Soft Thin (Metallic) Film to a Friction Pair in the Running-In Process," *Tribol. Lett.*, **11**, p 161.
(5) Bowden, F. P. and Tabor, D. (1942), *The Friction of Thin Films*, Australia Council for Scientific and Industrial Research, Melbourne (Bull. 145), p 23.
(6) Bowden, F. P. and Young, J. E. (1951), "Friction of Diamond, Graphite, and Carbon and the Influence of Surface Films," *Proc. R. Soc. Lond.*, p 444.
(7) Singer, I. L., Bolster, R. N., Wegand, J. and Fayeulle. S. (1990), "Hertzian Stress Contribution to Low Friction Behavior of Thin MoS_2 Coatings," *Appl. Phys. Lett.*, **57**, p 995.
(8) El-Sherbury, M. G. D. and Halling, J. (1976), "The Hertzian Contact of Surfaces Covered with Metallic Films," *Wear*, **40**, p 325.
(9) Leverson, R. C. (1974), "The Mechanics of Elastic Contact with Film-Covered Surfaces," *J. Appl. Phys.*, **45**, p 1041.
(10) Tian, H. and Saka, N. (1991), "Finite Element Analysis of an Elastic-Plastic Two-Layer Half-Space: Normal Contact," *Wear*, **148**, p 47.
(11) Matthewson, M. J. (1982), "The Effect of Thin Compliant Protective Coating on Hertzian Contact Stress," *J. Phys. D: Appl. Phys.*, **15**, p 237.
(12) Rabinowicz, E. (1967), "Variation of Friction and Wear of Solid Lubricant Films with Finite Thickness," *ASLE Trans.*, **10**, p 1.
(13) El Shafei, T. E. S., Arnell, R. D. and Halling, J. (1982), "An Experimental Study of the Hertzian Contact of Surfaces Covered by Soft Metal Films," *ASLE Trans.*, **26**, p 481.
(14) Finken, E. L. (1970), "Applicability of Greenwood-Williamson Theory to Film Covered Surfaces," *Wear*, **15**, p 291.
(15) Zhang, X. and Kato, K. (1996), "Friction Model of Thin Solid Lubrication," *J. Tribol.*, **118**, p 693.
(16) Ogilvy, J. A. (1993), "Predicting the Friction and Durability of MoS_2 Coatings Using a Numerical Contact Model," *Wear*, **160**, p 171.
(17) Wu, G., Gao, F., Kaltchev, M., Gutow, J., Mowlem, J., Schramm, W. C., Kotvis, P. V. and Tysoe, W. T. (2002), "An Investigation of the Tribological Properties of Thin KCl Films on Iron in Ultrahigh Vacuum: Modeling the Extreme-Pressure Lubricating Interface," *Wear*, **252**, p 595.
(18) Gao, F., Wu, G., Stacchiola, D., Kaltchev, M., Kotvis, P. V. and Tysoe, W. T. (2003), "The Tribological Properties of Monolayer KCl Films on Iron in Ultrahigh Vacuum: Modeling the Extreme-Pressure Lubricating Interface," *Tribol. Lett.*, **14**, p 99.
(19) Gao, F., Kotvis, P. V. and Tysoe, W. T. (2004), "Surface and Tribological Chemistry of Chlorine- and Sulfur-Containing Lubricant Additives," *Tribol. Int.*, **37**, p 87.
(20) Gao, F., Kotvis, P. V. and Tysoe, W. T. (2003), "The Frictional Properties of Thin Inorganic Halide Films on Iron Measured in Ultrahigh Vacuum," *Tribol. Lett.*, **15**, p 327.
(21) Gao, F., Kotvis, P. V. and Tysoe, W. T. (In press), "The Friction, Mobility and Transfer of Tribological Films: Potassium Chloride and Ferrous Chloride on Iron," *Wear*.
(22) Wytenburg, W. J. and Lambert, R. M. (1992), "Long-Lived Aluminum Evaporation Source for Controlled, Reproducible Deposition of Clean Ultrathin Films under Ultrahigh-Vacuum Conditions," *J. Vac. Sci. Technol. A, Vac. Surf. Films*, **10**, p 3579.
(23) National Institutes of Health, http://rsb.info.nih.gov/nih-image/
(24) Johnson, K. L. (2001), *Contact Mechanics*, Cambridge University Press, Cambridge.
(25) Greenwood, J. A. and Williamson, J. B. P. (1966), "Contact of Nominally Flat Surfaces," *Proc. R. Soc. A.*, **295**, p 300.
(26) Xie, Y. and Williams, J. A. (1996), "The Prediction of Friction and Wear When a Soft Surface Slides against a Harder Rough Surface," *Wear*, **196**, p 21.
(27) Moses, A. J. (1971), *Handbook of Electronic Materials, Vol. 1*, IFI/Plenum, New York.
(28) Musikant, S. (1985), *Optical Materials,* Marcel Dekker, New York.